# INFRASOUND AS A DEPTH DISCRIMINANT

Stephen J. Arrowsmith[1], Hans E. Hartse[1], Steven R. Taylor[2], Richard J. Stead[1], and Rod W. Whitaker[1]

Los Alamos National Laboratory[1] and Rocky Mountain Geophysics, LLC[2]

Sponsored by the National Nuclear Security Administration

Award No. DE-AC52-06NA25396/LA09-Depth-NDD02

## ABSTRACT

The identification of a signature relating depth to a remotely recorded infrasound signal requires a dataset of earthquakes, recorded infrasonically, with well-constrained depths. Although the premise is simple, five significant complications arise: (1) Earthquakes can generate infrasound via a variety of processes, which have occasionally been confused in past studies due to the complexity of the process; (2) mining explosions are efficient infrasound generators and can be mistaken for earthquakes; (3) coherent noise on infrasound arrays can be confused with transient signals; (4) atmospheric path effects must be adequately accounted for; and (5) seismic estimates of depth trade-off with origin time without a measurement in the near-epicentral region. This study provides a comprehensive framework for addressing these limitations, building on a focused study of the Wells, Nevada earthquake sequence that was performed as part of the previous year of this research effort (Arrowsmith et al., 2009). Such an approach is necessary to robustly identify a depth signature within a signal that incorporates various source, path, and receiver effects. In addition, we outline a complementary seismo-acoustic modeling approach, also being explored as part of this study, which should provide insight into the physical basis of an infrasonic depth signature.

## OBJECTIVES

The depth of an event is an important tool in event classification and is used in the Event Classification Matrix (ECM) as a discriminant. Seismic depths can be uncertain unless a seismometer happens to be located near the epicenter, because there is a trade-off between event depth and origin time in routine location algorithms. The fundamental objective of this research is to determine whether infrasound can be used to provide information on event depth. Towards this goal we aim to empirically search for a depth signature in real infrasound data. Coupled with this focus, we aim to model the generation of infrasound from earthquakes in order to provide an improved understanding of the physical basis of the generation of infrasound.

## RESEARCH ACCOMPLISHED

### Dataset

The completed dataset for this study comprises a regional component (Western US) and a global component.

*(a) Regional Dataset*

Arrowsmith et al. (2009) outlined the initial development of a dataset with the following requirements: (1) Each event must be recorded at >1 infrasound array, (2) each event must have accurate source constraints, and (3) a high-resolution atmospheric model must be available. The final regional dataset is shown in Figure 1 (care was taken to ensure earthquakes were not misidentified mine blasts; regions of mining activity are also depicted in Figure 1). From an initial dataset of 353 earthquakes (Figure 1), synchronous with data availability in our holdings at two or more arrays within 1500 km, we observed 7 earthquakes at multiple arrays (red stars in Figure 1), with magnitudes ranging from 3.7 to 5.8.

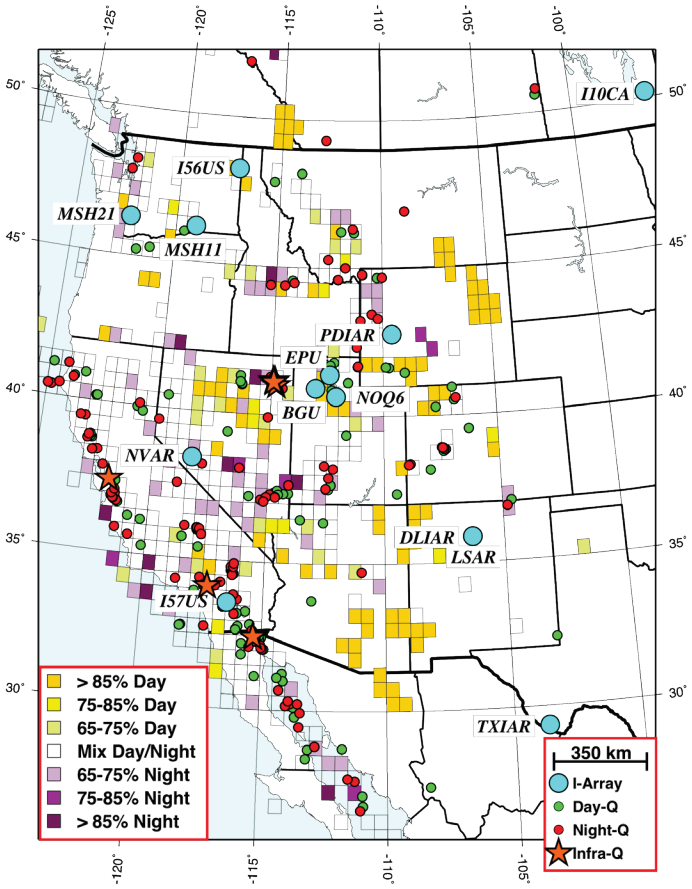


**Figure 1. Map of the regional dataset in the Western US. Red stars are detected earthquakes, green circles and red circles are undetected day and night earthquakes. Infrasound arrays in our database are depicted as blue circles.**

*(b) Global Dataset*

To extend the limited regional dataset, we have undertaken an extensive search for large earthquakes (M>5) in our global data holdings. By focusing on large earthquakes near infrasound arrays, we minimize the likelihood of mis-association (the purpose of constraint 1 above). Thus, we have compiled a list of earthquakes with the following constraints:

- Origin location between 100 and 400 km from any infrasound array;
- Mw > 5.0;
- Synchronous with data availability from the array.

The resultant catalog of earthquakes is plotted in Figure 2. We distinguish between shallow earthquakes and deep earthquakes using a depth boundary of 50 km. In total, there are 37 earthquakes that range in depth from 3 to 189 km. For each earthquake, we have obtained the USGS earthquake catalog information, the Harvard CMT solution (where available), and the G2S model specifications appropriate for the source-receiver path. These constraints provide a *starting point*, but are being refined upon as described in detail below.

The global dataset comprises earthquake swarms in South America, East Africa, and Japan (Figure 2). Working with earthquake swarms is advantageous, as outlined in more detail below, because the repeating source facilitates phase identification. Further, if a cluster of events is close enough in time and space, the individual events can be considered to have sampled the same atmosphere, removing the need for a path correction.

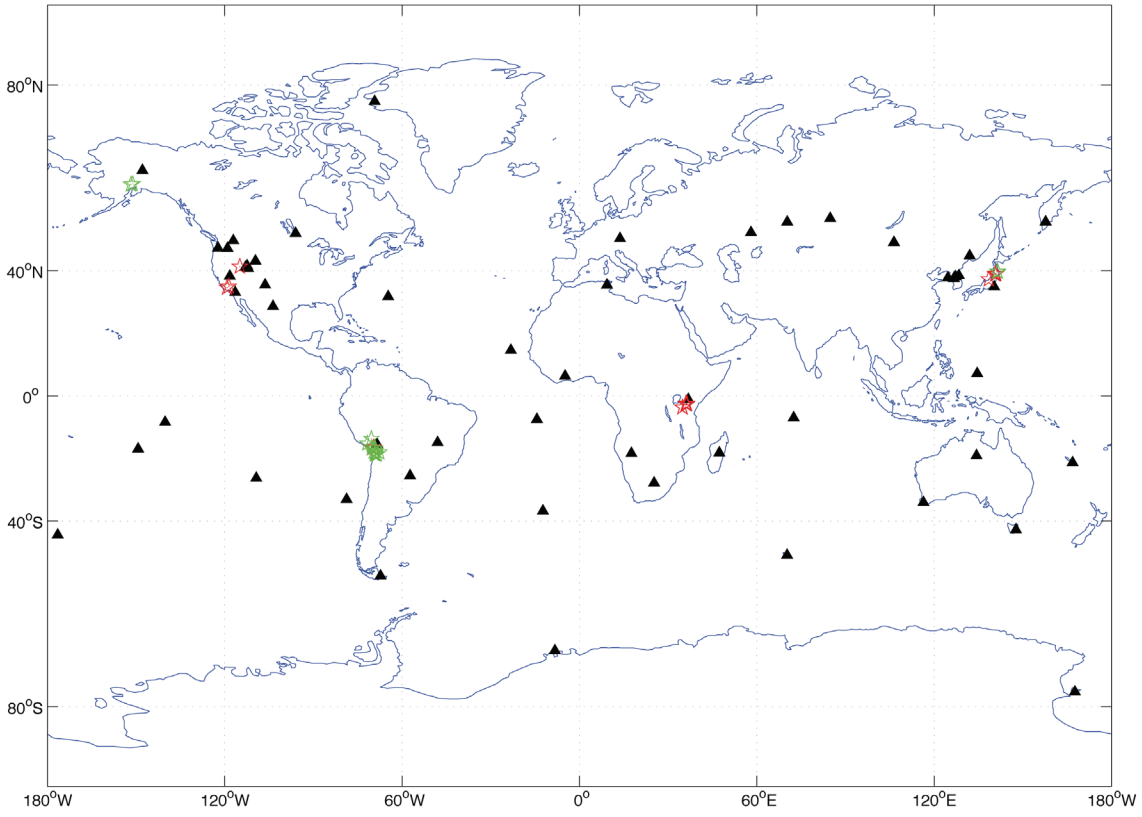


**Figure 2. Map showing the locations of infrasound arrays available for this study (black triangles) and earthquakes with M>5.0 at distances between 100 and 400 km from each array (stars). Waveform data has been obtained and stored for all earthquakes shown in this plot. Red stars denote shallow (< 50 km) earthquakes, while green stars denote deep (> 50 km) earthquakes.**

**Data Analysis**

An overall comparison of the detectability of shallow and deep earthquakes is given in Figure 3 (noting that this plot has been constructed for all earthquakes in the global dataset, i.e., M>5.0 and signals were detected at a single array at distances between 100 and 400 km). Based on this plot, two notable conclusions are made: (1) very deep earthquakes can generate infrasound, (2) the probability of detecting a shallow earthquake is >> 0.5 while the probability of detecting a deep earthquake is < 0.5. These findings indicate that infrasound has potential as a depth discriminant, but that further research is required to characterize the difference between infrasonic signatures from shallow and deep earthquakes.

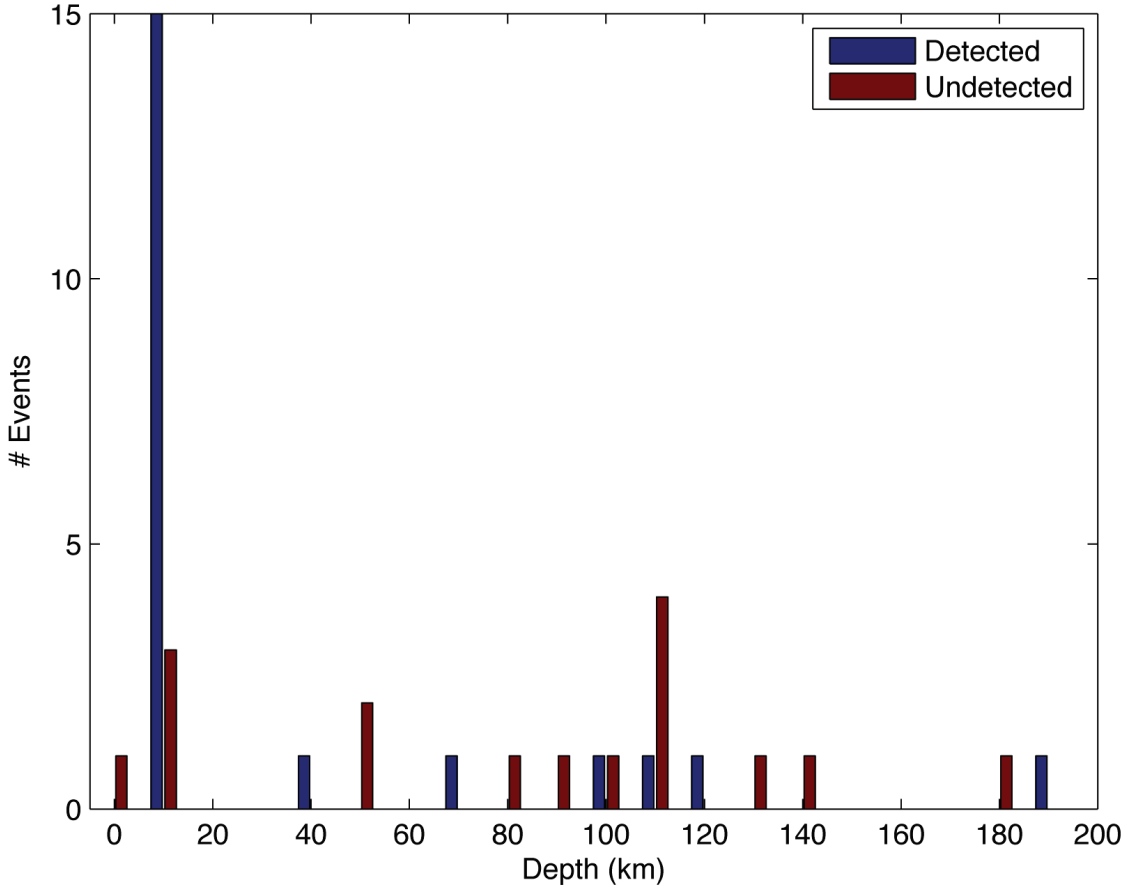


**Figure 3. Histogram providing a comparison between the depths of detected (blue) and undetected earthquakes (red). While a majority of shallow earthquakes at these ranges and magnitudes are detected, the majority of deep earthquakes are undetected. Further research is needed to characterize the difference between signals from detected shallow and deep earthquakes.**

A swarm of earthquakes in Tanzania provides a clear illustration of the effects of variations in source and path effects. As shown in Figure 4, while local infrasound (infrasound generated at the receiver by seismic waves) is similar from event to event, epicentral infrasound (which has propagated through the atmosphere) shows clear variations, reflecting the dynamic nature of the atmospheric path. While arrivals with group velocities of 0.27–0.31 km/s are persistent, later arriving signals with group velocities of ~0.25 km/s – which are much stronger in amplitude – are only observed for some of the events. This example clearly illustrates the value of using earthquake sequences (repeating sources), for identifying and separating different phases.

Preliminary measurements of these signals, and associated earthquake source parameters, are provided in Table 1 (noting that we are working on improving the earthquake source parameters as described in the next section). Peak-to-peak amplitudes, associated phase and group velocities, and periods, have been measured for the maximum

infrasound signal on each trace, discounting the local infrasound (Table 1). The component of the stratospheric wind from source to receiver, averaged between 45 and 55 km, is denoted $v_d$ and also provided in Table 1. Positive values of $v_d$ indicate that the wind component is in the direction of propagation, while negative values indicate that the wind component is in the opposite direction. Mutschlecner et al. (1999) developed an empirical formula for using this term to normalize for the effects of winds on the amplitudes of stratospheric returns. Using this formula, provided in Mutschlecner and Whitaker (2005), the winds normalized for the effects of distance and winds, $A_N$, are also provided in Table 1 for phases with stratospheric group velocity (0.27 – 0.31 km/s).

An example of an infrasound detection from a deep earthquake is provided in Figure 5. In this example, both local infrasound and epicentral infrasound are clearly detected—with backazimuths consistent with the great-circle backazimuth—above the background noise. The signal amplitudes are relatively low, but sufficient for reliable measurement by an analyst. This clear detection of a deep earthquake highlights the need to obtain an improved understanding of the generation of infrasound from earthquakes.

**Source/Path/Receiver effects**

One way in which this study aims to improve upon earlier studies is by improving the confidence with which we account for source, path, and receiver effects. The approach taken, relevant to each of these components, is described below.

*(a) Source Effects*

Studies by Mutschlecner and Whitaker (2005) and ReVelle (2005) utilized the USGS earthquake catalog to provide *a priori* information on earthquake magnitude, location, and depth. Here, we aim to determine high-resolution estimates of earthquake depth, in addition to mechanism, by modeling the seismic waveforms using a reflectivity method (Randall, 1989).

*(b) Path Effects*

Mutschlecner and Whitaker (2005) utilized available rocketsonde data to determine averaged zonal and meridional winds at elevations between 45 and 55 km. Due to the temporal and spatial sparseness of rocketsonde data, this required interpolation to obtain wind data suitable for a given location and time. Here, we aim to improve upon this correction by using the Ground-To-Space (G2S) model for the precise location and to the nearest hour. The use of earthquake sequences (repeating sources) also helps to better characterize and separate path effects.

*(c) Receiver Effects*

The goal here is to provide accurate and appropriate measurements that minimize the effect of ambient noise and are suitable for the purpose of depth estimation. The prior requirement is accomplished by making all measurements on the beam trace, and by only utilizing large earthquakes (M>5.0) to enhance signal/noise ratios. The latter requirement is more complex but should be based in part on a coupled modeling effort to determine what measurements would be representative of depth based on an improved understanding of the physical mechanism of infrasound generation (e.g., peak to peak amplitude, rms amplitude, period, duration, etc.)

**Modeling**

We plan to leverage R&D reported by Whitaker (2007, 2008, and 2009) on modeling the near-source infrasound generated by an underground source. Whitaker outlined the use of a Rayleigh Integral (RI) method, and a finite difference computational fluid dynamics program (CAVEAT), to predict the infrasound generated by an input ground acceleration model. Using a 3D finite difference code for the solid earth, E3D (Larsen and Schultz, 1995),we have begun to predict surface ground motions from earthquakes at two different depths (7 km and 15 km) and with three orthogonal source mechanisms (e.g., Figure 6). These ground motions will then provide the initial conditions for RI/CAVEAT. Through E3D-RI/CAVEAT, we hope to tie this modeling to the observational data described above.

As an example, Figure 6 shows the output from an E3D simulation for a pure strike-slip earthquake using the SCEC 1D model for the LA Basin (future research will utilize representative models for regions where we have data, such as Tanzania). The earthquake was located at 7 km depth. Displacement seismograms for a transect of hypothetical receivers clearly show the arrivals of P-wave, S-wave, and Surface wave energy.

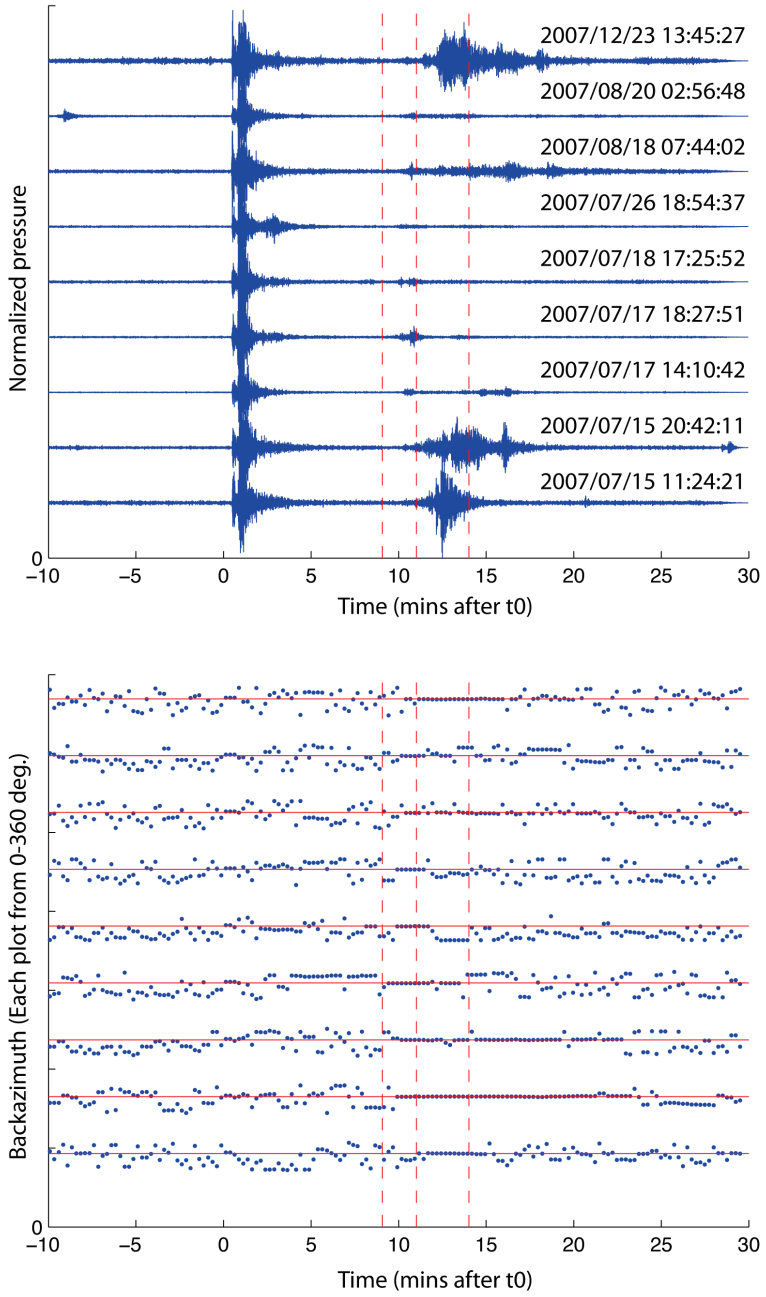


**Figure 4. Detailed plot showing the waveforms associated with detected earthquakes in Tanzania (top) and corresponding derived backazimuths, with great-circle backazimuths shown by horizontal red lines (bottom). Measurements of all earthquakes in this sequence are provided in Table 1. Dashed red lines (vertical) indicate group velocities of 0.34, 0.28, and 0.22 km/s, assuming the source of infrasound corresponds to the origin time.**

**Table 1. Summary of observations from Tanzania. Italicized earthquakes are of unknown phase.**

| Origin Time | Location | Mw | Depth (km) | Slip (°) | d (km) | A (Pa) | $v_d$ (m/s) | $A_N$ | T (s) | $v_p$ (m/s) | $v_g$ (m/s) |
|---|---|---|---|---|---|---|---|---|---|---|---|
| *2007/07/15 11:24:21* | *-2.93, 36.24* | *5.3* | *17.9* | *57.0* | *198.7* | *0.192* | *6.72* | | *0.65* | *0.34* | *0.26* |
| *2007/07/15 20:42:11* | *-2.88, 36.16* | *5.4* | *12.0* | *80.0* | *196.6* | *0.105* | *5.01* | | *0.83* | *0.34* | *0.25* |
| 2007/07/17 14:10:42 | -2.73, 36.36 | 5.9 | 12.0 | 86.5 | 173.4 | 0.059 | -0.13 | 0.0047 | 1.17 | 0.35 | 0.28 |
| 2007/07/17 18:27:51 | -2.78, 36.19 | 5.3 | 12.0 | 89.0 | 185.1 | 0.105 | -1.39 | 0.0096 | 0.59 | 0.35 | 0.29 |
| 2007/07/18 17:25:52 | -2.77, 36.09 | 5.1 | 12.4 | 81.5 | 188.6 | 0.033 | 2.38 | 0.0027 | 1.10 | 0.35 | 0.31 |
| 2007/07/26 18:54:37 | -2.68, 36.01 | 5.2 | 17.0 | 65.0 | 183.9 | 0.020 | -7.31 | 0.0023 | 0.72 | 0.35 | 0.30 |
| 2007/08/18 07:44:02 | -2.83, 36.21 | 5.2 | 12.0 | 82.0 | 189.4 | 0.034 | 3.50 | 0.0026 | 1.64 | 0.35 | 0.29 |
| 2007/08/20 02:56:48 | -2.71, 36.29 | 5.4 | 12.0 | 83.5 | 173.8 | 0.032 | 0.70 | 0.0025 | 0.60 | 0.35 | 0.27 |
| *2007/12/23 13:45:27* | *-2.78, 36.20* | *5.2* | *12.3* | *81.5* | *184.7* | *0.333* | *-10.34* | | *0.74* | *0.36* | *0.25* |

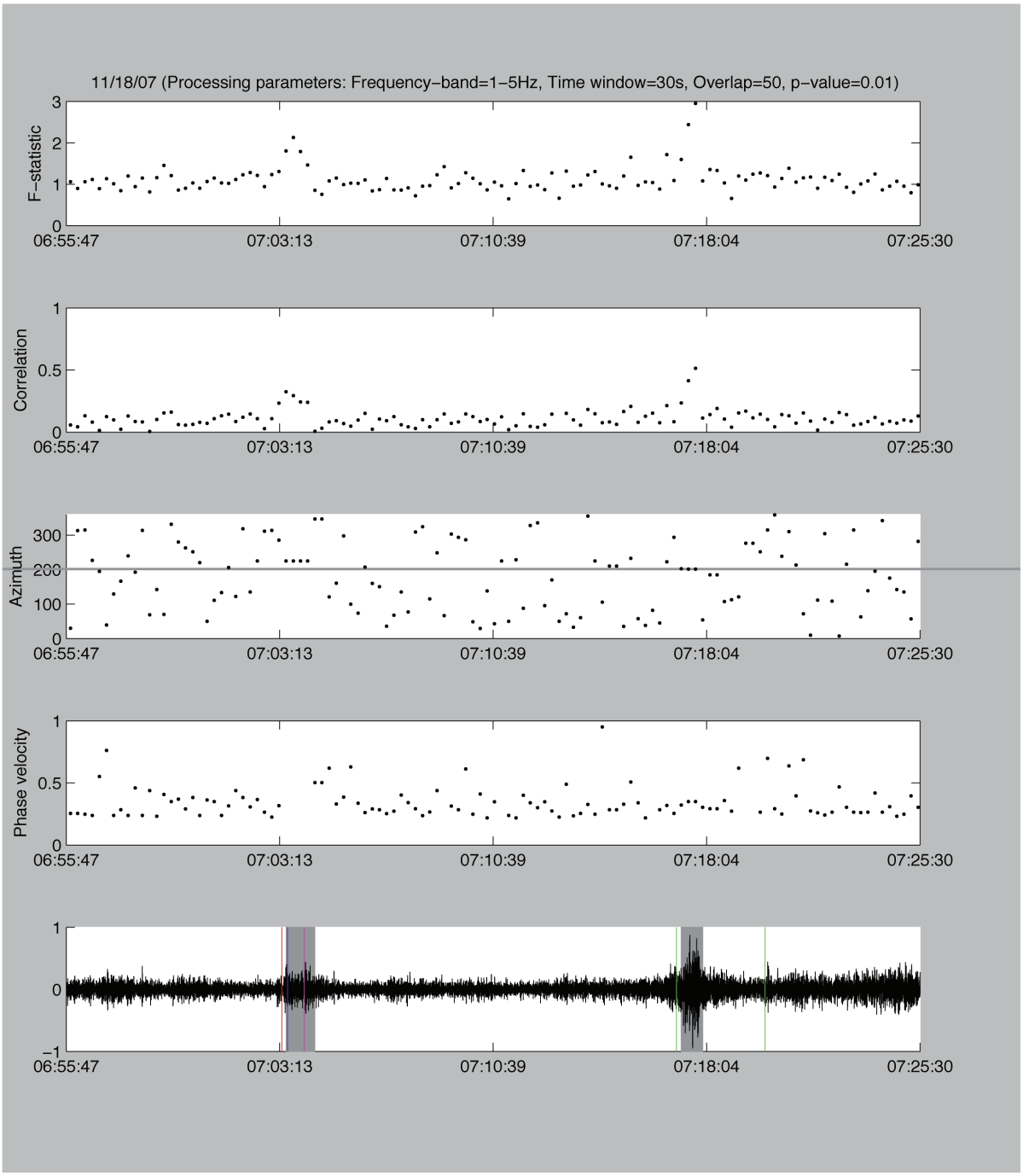


**Figure 5.** ***InfraMonitor*** **plot showing the normalized beam trace (bottom panel) and derived waveform parameters (top four panels) for a deep earthquake (Depth = 98.4 km) recorded at the I08BO array in Bolivia. Gray boxes denote automatic detections corresponding to the arrival of the seismic wave (left) and stratospheric infrasound (right).**

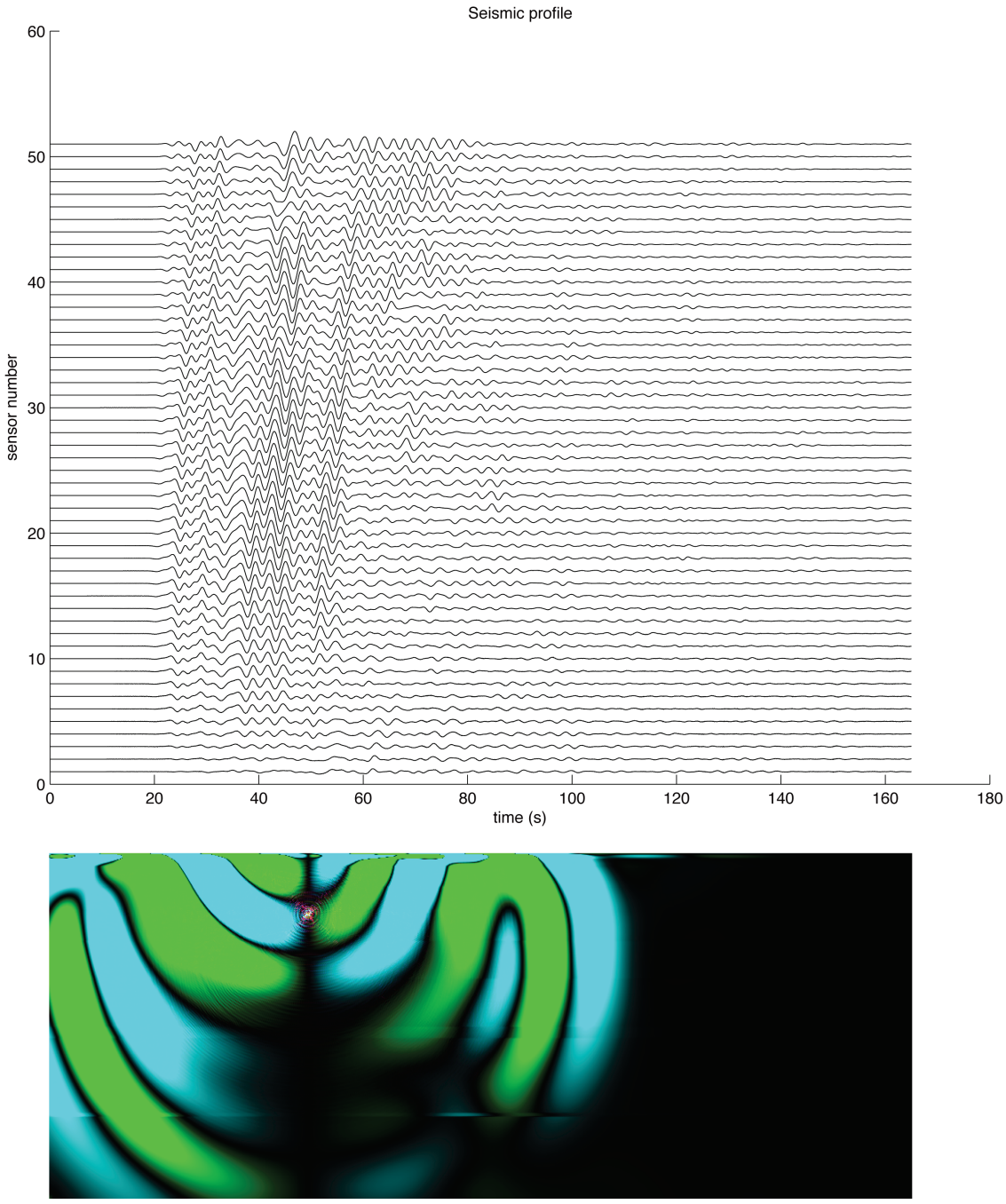


**Figure 6. Illustration of seismic E3D modeling. Bottom panel is a snapshot of the model at a given time, for a pure strike-slip earthquake at 7 km depth. A simple 1D velocity model has been used, representative of the LA Basin. Green and blue colors represent positive and negative S-wave energy. Top panel is a transect over the surface showing predicted ground displacement as a function of time at a series of hypothetical receivers.**

## CONCLUSIONS AND RECOMMENDATIONS

This paper is a report on continuing progress towards an infrasonic depth discriminant. We have completed the acquisition of a high-quality dataset comprising both regional (Western US) and global components. An analysis of detectability highlights the fact that very deep earthquakes can generate infrasound, but that the probability of detection for shallow earthquakes (depth < 50 km) is much higher than for deeper earthquakes, where only relatively few events are detected. We highlight the utility of earthquake sequences for providing reliable phase identification through analysis of the variability of the repeating source. We discuss steps that are being taken to better constrain source, path, and receiver effects. Finally, we report on the initial modeling R&D, which utilizes a seismo-acoustic modeling scheme that combines a seismic finite difference code (E3D) with techniques for converting ground accelerations to acoustic pressure in the near field.

## REFERENCES

Arrowsmith, S. J., H. E. Hartse, G. E. Randall, and S. R. Taylor (2009). Infrasound as a Depth Discriminant: Construction of a Unique Dataset and Preliminary Analyses, in *Proceedings of the* 2009 Monitoring Research Review: Ground-Based Nuclear Explosion Technologies, LA-UR-09-05276, Vol. 2, pp. 697–705.

Larsen, S., and C. A. Schultz (1995). ELAS3D: 2D/3D elastic finite-difference wave propagation code, Lawrence Livermore National Laboratory Technical Report No. UCRL-MA-121792.

Mutschlecner, J. P., R. W. Whitaker, and L. H. Auer (1999). An empirical study of infrasound propagation, Tech. Rep. LA-13620-MS, Los Alamos Natl. Lab., Los Alamos, N.M.

Mutschlecner, J. P., and R. W. Whitaker (2005). Infrasound from earthquakes, *J. Geophys. Res*. 110: doi:10.1029/2004JD005067.

Randall, G. E. (1989). Efficient calculation of differential seismograms for lithospheric receiver functions, *Geophys. J. Int*. 99: 469–481.

ReVelle, D. O. (2005). Additional Infrasonic Studies of Earthquakes and Mining Blasts Discrimination, in *Proceedings of the 27th Seismic Research Review: Ground-Based Nuclear Explosion Monitoring Technologies*, LA-UR-05-6407, Vol. 2, pp. 845–854.

Whitaker, R. W. (2007). Infrasound Signals as Basis for Event Discriminants, in Proceedings of the 29th Monitoring Research Review:Ground-Based Nuclear Explosion Monitoring Technologies, LA-UR-07-5613, Vol. 2, pp. 905–913.

Whitaker, R. W. (2008). Infrasound Signals from Ground-Motion Sources, in *Proceedings of the 30th Monitoring Research Review: Ground-Based Nuclear Explosion Monitoring Technologies*, LA-UR-08-05261, Vol. 2, pp. 912–920.

Whitaker, R. W. (2009). Infrasound Signals from Ground Motion Sources, in *Proceedings of the 2009 Monitoring Research Review: Ground-Based Nuclear Explosion Monitoring Technologies*, LA-UR-09-05276, Vol.2, pp. 750–758.